Sustainable Energy & Fuels

Accepted Manuscript

This article can be cited before page numbers have been issued, to do this please use: N. S, P. Sudhagar and Y. S. Kang, *Sustainable Energy Fuels*, 2017, DOI: 10.1039/C7SE00292K.

This is an Accepted Manuscript, which has been through the Royal Society of Chemistry peer review process and has been accepted for publication.

Accepted Manuscripts are published online shortly after acceptance, before technical editing, formatting and proof reading. Using this free service, authors can make their results available to the community, in citable form, before we publish the edited article. We will replace this Accepted Manuscript with the edited and formatted Advance Article as soon as it is available.

You can find more information about Accepted Manuscripts in the author guidelines.

Please note that technical editing may introduce minor changes to the text and/or graphics, which may alter content. The journal's standard Terms & Conditions and the ethical guidelines, outlined in our author and reviewer resource centre, still apply. In no event shall the Royal Society of Chemistry be held responsible for any errors or omissions in this Accepted Manuscript or any consequences arising from the use of any information it contains.

ROYAL SOCIETY OF CHEMISTRY

rsc.li/sustainable-energy

View Article Online
DOI: 10.1039/C7SE00292K

Sustainable Energy & Fuels

COMMUNICATION

Synthesising chain-like, interconnected Pt nanoparticles using tubular halloysite clay template for efficient counter electrode in dye-sensitised solar cells

Received 00th January 20xx,
Accepted 00th January 20xx

DOI: 10.1039/x0xx00000x

www.rsc.org/

S. Nagarajan,[a,b] Sudhagar Pitchaimuthu[a,c *] and Yong Soo Kang[a*]

We report an inexpensive fabrication route of mesoporous counter electrode, made of chain-like Pt nanoparticles using tubular halloysite clay template. Pre-coated halloysite tube (HT) onto a conducting substrate acts as material synthesising platform for highly interconnected chain-like Pt nanostructure. The Pt-HT composite counter electrode shows effective electrolyte interaction, and high catalytic activity towards tri-iodide reduction. As a result, Pt-HT counter electrode based dye-sensitised solar cells exhibits high energy conversion efficiency of 9.5% than the flat-type Pt film based counter electrode (8.2%) using liquid-type electrolyte.

Nanoscale catalyst substance possesses high specific surface area and surface energy, which lead to high catalytic activity. Recently, nanostructured catalyst electrodes are of interest in several industrial applications including energy conversion, energy storage, biomedical, and water purification systems.[1-3] Numerous synthetic routes are proposed to prepare nanoscale catalyst physically or chemically. However, simple and low-cost synthetic routes have been ever demanding to reduce the fabrication cost and to avoid complex experimental procedure towards large scale industrial deployment. Template-assisted method is a cutting edge chemical route for synthesising nanoscale catalyst in large scale.[4] The soft templates involved in the material synthesis offer a platform to obtain desired morphology, selective crystalline facet and mesoporous structures. To date, a wide range of soft templates including organic polymer,[5, 6] carbon nanotube,[7] metal oxide,[8] and clay[9] have been proposed. Among them, naturally available clay material is easy to handle and low-cost for large scale synthesis.

The halloysite clay [$Al_2Si_2O_5(OH)_4{\cdot}2H_2O$], a hydrated, layered aluminosilicate is a natural mineral consisting of hollow cylinders with multiple layers and submicrometer dimension.[10] The mismatch between the oxygen-sharing tetrahedral SiO_4 sheet and its adjacent octahedral AlO_6 sheet drives the multi roll wrapping and thus forms tubular shape halloysite clay.[11] These naturally available halloysite nanoscale tubes (HT) exhibits unique physical and chemical features of relatively high specific surface area, high porosity, and high cation-exchange capacity. Owing to their biocompatible nature, it has been widely applied in biomedical drug delivery applications.[12-14] The other interesting features such as high porosity, large surface area, and strong absorbability make HT a promising soft template for various applications such as nanoparticle synthesis,[9, 15] water treatment,[16] oil-spill recovery,[17] and energy storage devices[18]. Despite the advantageous of HT, less attention has been paid in nanoparticle synthesis because an additional process is required to separate resultant nanoparticles from their mixture with template. However, we can revisit implementation of HT in nanomaterial synthesis where the removal of template is not necessary. For instance, pre-coated HT onto conducting substrate can serve as thick mesoporous scaffold for supporting spatially distributed nanoparticle synthesis. Compare to flat type nanoparticle thin film coating, these spatially distributed nanoparticles could result high electrode/electrolyte interfaces in electrochemical based devices. In this view, the HT clay coated Pt nanoparticle coated electrode could be an appropriate choice for counter electrode application in dye-sensitised solar cells (DSSCs). It is anticipated that spatially distributed HT clay framework afford large pore channel that could act as backbone scaffold for spatial growth of target Pt catalyst material compare to conventional flat-type counter electrode. In addition, the mesopore structured HT backbone scaffold may facilitate the electrolyte percolation through the entire counter electrode.
The noble metal, Pt has been extensively utilised as a counter electrode component in (DSSCs).[19] The unique features of Pt

[a] Department of Energy Engineering, Hanyang University, Seoul, South Korea. Email: Kangys@hanyang.ac.kr
[b] Department of Chemistry, Manonmaniam Sundaranar University, Tamilnadu, India
[c] Multifunctional Photocatalyst and Coating Group, SPECIFIC, College of Engineering, Swansea University (Bay Campus), Fabian way, Crymlyn Burrows, Swansea SA1 8EN, United Kingdom (S.Pitchaimuthu@swansea.ac.uk; vedichi@gmail.com)
† Footnotes relating to the title and/or authors should appear here.
Electronic Supplementary Information (ESI) available: [Experimental details, SEM, TEM, and equivalent circuit]. See DOI: 10.1039/x0xx00000x

View Article Online
DOI: 10.1039/C7SE00292K

are its high catalytic activity, excellent chemical stability, less redox potential for tri-iodide reduction and therefore promotes Pt as a ubiquitous electro catalyst in DSSCs.[20] In general, Pt has been applied in the form of thin film mostly 2-5 nm as is enough to perform the effective trioxide reduction in liquid electrolyte. The less viscous nature of the liquid electrolyte eventually results in more feasible interaction with thin Pt surface. But, in the case of highly viscous solid electrolyte, filling of narrow pores in nano-structured photoanode with redox carriers (I^-/I_3^-) is often difficult. This could severely hinder to improve the overall conversion efficiency of the DSSCs. To enhance the counter electrode/solid electrolyte interfacial interactions, an impregnated or mesoporous structured catalysts are introduced in DSSCs. For instance, Li et. al. demonstrated vertically grown Pt nano-grass counter electrode. It exhibited 12% high photo conversion efficiency than conventional flat type Pt film based counter electrode.[21] Similarly, 1-D nanostructures (nanofiber, nanoflower, nano-urchin) based Pt counter electrodes has been demonstrated in DSSCs.[22-24] These reports clearly explored that spatially grown or elongated Pt nanostructures promote the interfacial contact with electrolyte. However, complicated synthesis route and low quantity of yield often challenges their large-scale synthesis.

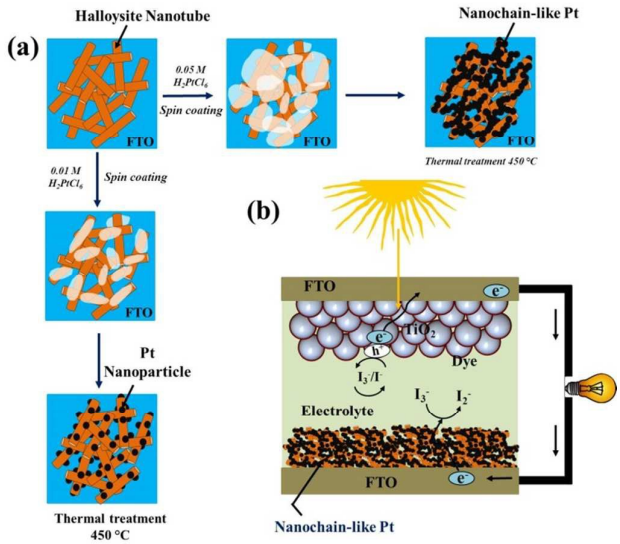

Scheme 1. Schematic illustration of different experimental stages in HNT-PT composite synthesis; (b) DSSC device architecture with HNT-Pt counter electrode.

Herein, we propose a facile synthesis of chain-like Pt nanoparticles using HT backbone template. To understand the Pt nanoparticle growth mechanism, the concentration of the Pt precursor (H_2PtCl_6) was varied from 0.01 to 0.05 M (**See experimental details in supporting information S1**). The different experimental stages of HT-assisted Pt nanoparticle synthesis are illustrated in **Scheme 1**. Pt precursor solution was first deposited onto the HT layer pre-coated on the fluorinated tin oxide (FTO) substrate (**Scheme 1a**). Subsequently this film was sintered at 450 °C and ambient atmosphere. During sintering process, the Pt precursor was reduced into nanoparticle onto the HT surface.

The detailed electrocatlytic performance of Pt-HT composite was studied and compared with HT-free Pt film. Also their counter electrode performance was examined in liquid electrolyte based dye-sensitised solar cells. The schematic structure of DSSCs using Pt-HT counter electrode is depicted in **Scheme 1b**. It is anticipated that thick (~3 micron), mesoporous Pt-HT counter electrode might allow more electrolyte species into the entire electrode geometry, thus increase electrode/electrolyte interfaces, compared to flat, HT-free Pt film. In addition, the travelling distance of redox shuttle (I^-/I_3^-) between photoanode and counter electrode can be reduced by the thick Pt-HT counter electrode, which may supporting the dye-regeneration rate at photoanode.

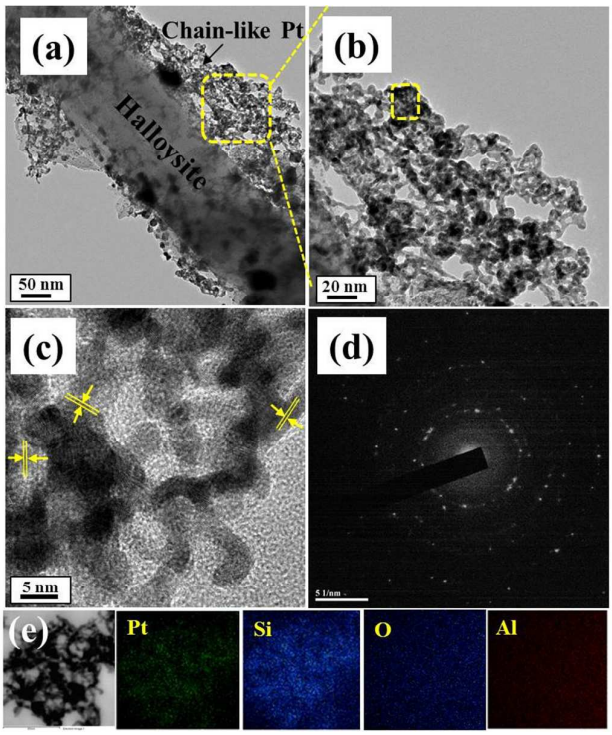

Figure 1. (a) HRTEM images of Pt-HT (0.03 M) at 50 nm scale and (b) enlarged image of dotted area noted in Figure 1(a) at 20 nm scale; (c) high resolution lattice image of Pt chain-like structure recorded from Pt-HT (0.03 M) sample and (d) corresponding selected area diffraction pattern (SAED) result; (e) elemental mapping of Pt, Si, O, and Al species from scanned area of Figure 1(e).

The surface morphology of Pt-HT composite for different Pt precursor concentration was studied by scanning electron microscopy (**Figure S2**). From **Figure S2 (a)-(c)** it is observed that the density of spatial distribution of Pt nanoparticles directly depend on the Pt precursor concentration (**Figure S2).** At the high concentration of 0.03 M, highly interconnected chain-like Pt nanoparticles are visible in the Pt-HT sample. This reveals the influence of the Pt precursor concentration on morphology of the Pt nanoparticle. To further understand the growth mechanism of Pt nanoparticle onto the HT surface, we

View Article Online
DOI: 10.1039/C7SE00292K

have recorded the high-resolution transmission electron microscope (HRTEM) images (**Figure 1 and Figure S3**).

Figure S2 and S3 shows the Pt nanoparticles deposited on the HT surface. Their size is in the range from ~5 nm to ~50 nm at the low Pt precursor concentration (0.01 M). Further increasing the Pt precursor concentration (0.03 M), the size and the amount of the Pt nanoparticle were increased significantly, suggesting that they may be spatially interconnected to form chain-like structure on the HT surface (**Figure 1 (a) and (b)**). In close proximity at 5 nm scale (**Figure 1c**), the lattice fringe of the Pt nanoparticles showed 0.19 nm in diameter between two lattice channel,[25] implying (101) crystalline plane of Pt. The SAED pattern (**Figure 1d**) further endorses the highly crystalline nature of Pt. The elemental mappings for the chain-like nanoparticles are presented in **Figure 1(e)**. The observed Pt, Al, Si and O elements advocated that the chain-like particles would be Pt nanocrystals. From these observations, we believe that the HT surface acts as a substrate for Pt seed layer growth, which also facilitate adjacent Pt particles to fuse into each other and thus the chain-like structure is stabilized. Further, the Pt precursor concentration has increased to 0.05 M resultant Pt nanoparticle are agglomerated (**Figure S3 (c)**).

Prior to the DSSCs assembly, the electrocatalytic activity of the as-synthesised Pt-HT composite counter electrode was evaluated in tri-iodide reduction reaction. The cyclic voltammogram (CV) results are presented in **Figure 2 (a)**. The conventional Pt thin film counter electrode coated on a FTO electrode exhibited two peaks:

The peak at lower potential ~-0.24 V vs Ag/AgCl is attributed to reduction of tri-iodide.[26]

$I_3^- + 2e^- \leftrightarrow 3I^-$ (1)

The peak exhibiting at positive potential of ~0.43 V vs Ag/AgCl is associated with the oxidation reaction.

$3I_2^- + 2e^- \rightarrow 2I_3^-$ (2)

A distinguished peak observed in negative potential region ~-0.02 V vs Ag/AgCl of Pt-Ht (0.03 M) electrode reveals that less operating potential is adequate to drive the trioxide reduction (Eqn. 1), compared to the conventional Pt film. In the case of Pt-HT (0.01 M) electrode, the reduction potential is slightly increased to -0.1 V vs Ag/AgCl. As discussed in the TEM results the Pt-HT (0.01 M) film encompasses the less quantity of the Pt nanoparticle loading as well as randomly coated inhomogeneous Pt nanoparticles onto the HT surface. This could result in relatively less electron conductivity and thus exhibited poorer electrocatalytic activity, compared to the Pt-HT (0.03 M) electrode. On the other hand, the Pt-HT (0.05 M) electrode with the highest Pt concentration also resulted in poorer electrocatalytic activity, presumably due to the aggregation of Pt nanoparticles and thus the reduced active surface area for catalytic reaction. In general, the catalytic activity of the counter electrode can be qualitatively evaluated from two parameters from C-V plots a) "peak separation" (ΔE_p) and (b) "cathodic peak current density" (I_p) observed at more negative potential. The ΔE_p value is related with the kinetic redox capability of the cathode for I^-/I_3^-. Therefore, the smaller ΔE_p infers the better electrocatalytic ability of a counter electrode. From **Figure 2a**, the estimated ΔE_p value of the Pt-HT (0.03 M) electrode is ~0.303 V, which is twofold lesser than that of the conventional Pt film (ΔE_p~ 0.70 V). These results imply the advantage of Pt-HT composite as an electro-catalytic counter electrode in DSSCs.

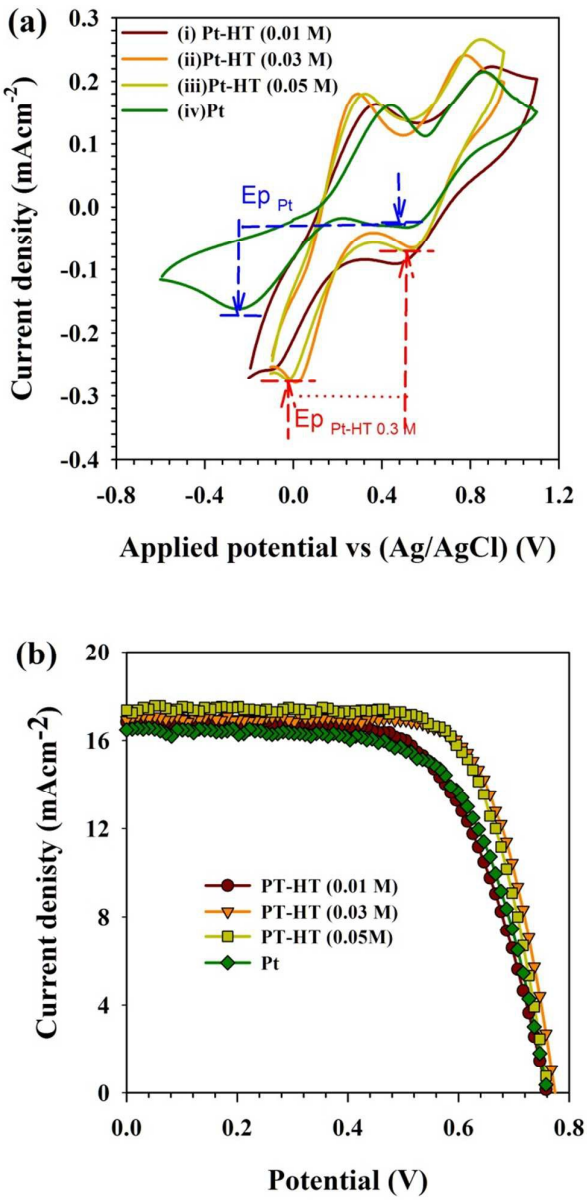

Figure 2. (a) cyclic voltammograms of Pt-HT electrodes by varying the concentration of the precursor solution and the Pt film coated FTO substrate (Note that the electrolyte containing methoxypropionitrile solvent with 10 mM LiI, 1 mM I_2 and 0.1 M $LiClO_4$ measured at a fixed scan rate of 100 $mV.s^{-1}$); (b) J-V plot of dye-sensitized solar cells fabricated with different counter electrodes (Pt-HTs and Pt.

The photovoltaic performance of the Pt-HT composite counter electrodes was characterized in dye-sensitized solar cells

View Article Online
DOI: 10.1039/C7SE00292K

(DSSCs) (**Scheme 1b**). First, these electrodes were examined with liquid-type electrolyte as it has less complexity in understanding the device performance. The *J-V* measurement results are presented in **Figure 2(b)**. The photovoltaic parameters derived from **Figure 2(b)** are enlisted in **Table 1**. Under identical experimental conditions, the Pt-HT (0.03) counter electrode showed higher photocurrent density of J_{sc} = 16.9 mAcm^{-2} than the other Pt-HT composite electrodes as well as the HT-free Pt film. This enhancement can be attributed to several advantages of the Pt-HT (0.03) counter electrode such as a) high catalytic activity in tri-iodide reduction as discussed in **Figure 2(a)**, and b) effective electrolyte/electrolyte interaction. As a result, the Pt-HT (0.03) cell performed high photo conversion efficiency (PCE) η=9.5% with open circuit voltage (V_{oc}) 0.77 V and fill factor (*FF*) 0.72. Compared to the HT-free Pt film, the Pt-HT (0.03) composite showed 115% improvement in PCE. This is mainly ascribed to the enhancement of *FF* by modifying the Pt nanoparticle growth condition and the counter electrode architecture (**Scheme 1b**). The reproducibility of these counter electrodes were tested in three batches and the photovoltaic results were summarised in **Figure S4**. It is worth to discuss that how the fill factor plays a key role in determining PCE of the device.

Table 1. Photovoltaic parameters of DSSCs with different counter electrodes. (Measured under 100 mW cm^{-2}, AM 1.5 G illumination, shadow mask: 0.25 cm^{-2})

Counter Electrode	Voc (V)	Jsc/ (mAcm^{-2})	FF	η (%)
Pt-HT (0.01)	0.759	16.42	0.709	8.8
Pt-HT (0.03)	0.774	16.93	0.728	9.5
Pt-HT (0.05)	0.766	16.75	0.716	9.1
Pt	0.759	16.82	0.643	8.2

In general, the fill factor of DSSCs is governed by the internal series resistance (R_{se}) of the device, which associates sheet resistance of both electrodes substrate (R_{sub}), charge transfer resistance at both electrode/electrolyte interfaces (R_{ct}) as well as diffusion resistance through the electrolyte (R_{diff}).[27, 28]

$$R_{se} = R_{sub} + R_{ct} + R_{diff} \quad (3)$$

By following Eqn.3, the R_{ct} value of counter electrode can explain the influence of its structure on the fill factor of the device. The electrochemical impedance spectroscopy is a unique tool to study the charge transfer characteristics, the origin of traps, and stability of the electrode while keeping in the electrolyte unchanged.[29-32] The Nyquist plots for different counter electrodes (dummy cell configuration) are obtained in the frequency range of 1 Hz to 1MHz at 0.75 V vs Ag/AgCl with an AC amplitude of 10 mV under AM 1.5G illumination. The Nyquist plot is further simulated with the equivalent circuit as presented in the **Figure S5**. In the equivalent circuit, R_s indicates the sheet resistance of the charge collector (FTO), CPE indicates the constant phase element, and R_{ct} indicates twice the time of charge transfer resistance. Strikingly, the Pt-HT (0.03) electrode showed R_{ct} ~0.5 Ωcm^{-2}, which is six fold lesser than that of the conventional HT-free Pt film (R_{ct} ~3.5 Ωcm^{-2}). It is clear that the chain-like Pt nanoparticles on the mesopores HT framework promote the interconnectivity between the Pt nanoparticles that enhances the electron conductivity of the electrode and thus, reduced the charge transfer resistance at electrode/electrolyte interfaces. In accord to Eqn. 1 the extremely less R_{ct} value of Pt-HT (0.03M) seems to be responsible for high fill factor in this device. The less loading of the Pt nanoparticles for Pt-HT (0.01 M) resulted in high R_{ct} ~8.3 Ωcm^{-2}, as expected, which slightly reduce both J_{sc} and *FF* of the device.

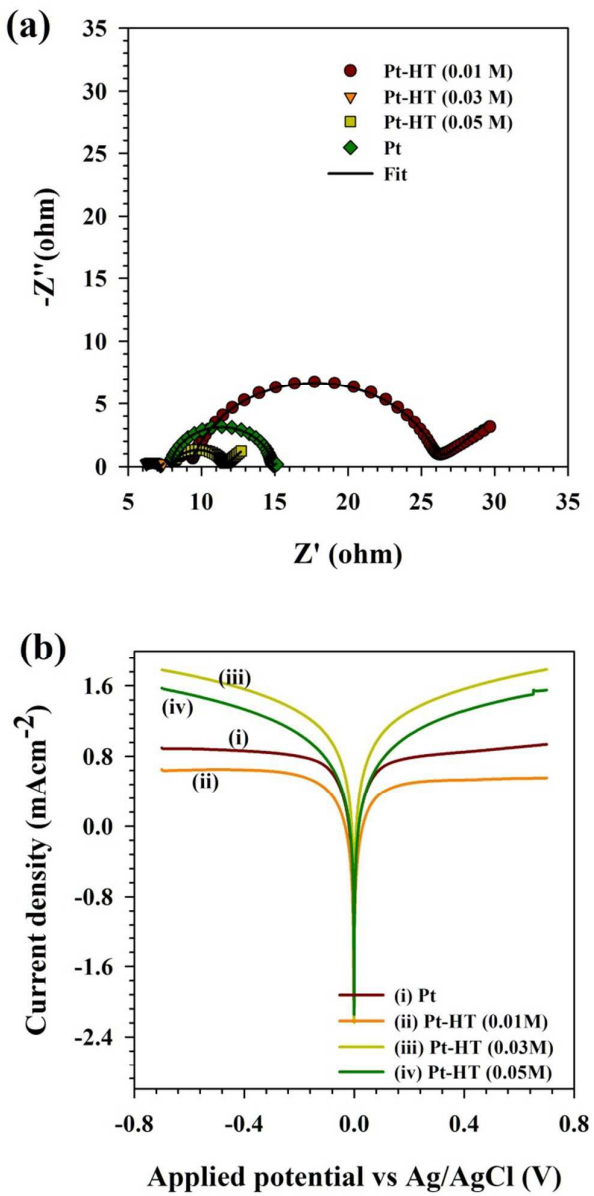

Figure 3. (a) Nyquist plots of dye-sensitized solar cells with different counter electrodes [the measurements were carried out under 100 mWcm^{-2} illumination and AM 1.5; (b) Tafel plots of different counter electrodes.

View Article Online
DOI: 10.1039/C7SE00292K

The interfacial charge-transfer properties of I_3^-/I^- redox shuttle at different counter electrode were studied through Tafel plots. The Tafel plots were recorded using the symmetric cell configuration (electrode/electrolyte/electrode). The resultant Tafel plots in **Figure 3(b)** presents that the Pt-HT (0.03) electrode showed high exchange current density (J_0) than the conventional HT-free Pt film as well as the other Pt-HT electrodes. The higher the J_0 value, the better the catalytic activity towards I_3^- reduction. This is in good agreement with CV and EIS results in **Figure 2(a) and Figure 3 (a)**. Though the Pt-HT (0.01) showed apparently high charge transfer resistance and lower exchange current density it results slightly high photoelectric conversion efficiency than Pt. This discrepancy may arise from the difference in experiment environment. For instance, the JV plots were measured using DSSCs device architecture (Photoanode/electrolyte/Pt). In the case of Tafel and impedance (Nyquist) plots were obtained from dummy cell (Pt/electrolyte/Pt).

From the above discussion, it is clear that the Pt-HT (0.03M) electrode showed multiple advantages such as high electro catalytic activity, effective electrolyte interaction, less interfacial charge-transfer resistance at electrode/electrolyte interfaces than the conventional counter electrode of the HT-free Pt film. These results encourages to applying this counter electrode further in solid-state electrolyte. It is anticipated that mesoporous channels at counter electrode facilitate the percolation of even highly viscous electrolyte[33] and also the better interfacial contact with even solid state electrolyte.

Conclusions

In summary, we have demonstrated the chain-like Pt nanoparticles using tubular halloysite clay template. The method to prepare Pt nanoparticles grown onto a pre-coated HT clay mesoporous electrode showed a promising route for enhanced interaction between the electrolyte/counter electrode with higher electro catalytic activity and less charge transfer resistance. This Pt-HT composite electrode can be widely applied as anode/cathode component for energy conversion and storage devices. In addition, generic synthesis route of highly interconnected catalytic nanoparticles can also be utilized in deriving nanoscale metal, metal oxide, metal sulphide and carbonaceous materials.

Notes and references

SN would like to acknowledge Ramalingaswami re-entry Fellowship from DBT (BT/RLF/Re-entry/40/2015), India for supporting the PI. SP acknowledges Welsh Government and European Regional Development Fund (ERDF) for partial support through Sêr Cymru II-Rising Star Fellowship program.

1. Y. Li and G. A. Somorjai, *Nano Letters*, 2010, **10**, 2289-2295.
2. G. G. Wallace, J. Chen, A. J. Mozer, M. Forsyth, D. R. MacFarlane and C. Wang, *Materials Today*, 2009, **12**, 20-27.
3. N. Sharma, H. Ojha, A. Bharadwaj, D. P. Pathak and R. K. Sharma, *RSC Advances*, 2015, **5**, 53381-53403.
4. C. R. Martin, *Chemistry of Materials*, 1996, **8**, 1739-1746.
5. J. R. Capadona, O. Van Den Berg, L. A. Capadona, M. Schroeter, S. J. Rowan, D. J. Tyler and C. Weder, *Nat Nano*, 2007, **2**, 765-769.
6. J. Liu, T. Yang, D.-W. Wang, G. Q. Lu, D. Zhao and S. Z. Qiao, *Nature Communications*, 2013, **4**, 2798.
7. P. M. Ajayan, O. Stephan, P. Redlich and C. Colliex, *Nature*, 1995, **375**, 564-567.
8. X. Xiao, H. Song, S. Lin, Y. Zhou, X. Zhan, Z. Hu, Q. Zhang, J. Sun, B. Yang, T. Li, L. Jiao, J. Zhou, J. Tang and Y. Gogotsi, *Nature Communications*, 2016, **7**, 11296.
9. E. Abdullayev, K. Sakakibara, K. Okamoto, W. Wei, K. Ariga and Y. Lvov, *ACS Applied Materials & Interfaces*, 2011, **3**, 4040-4046.
10. E. Joussein, S. Petit, J. Churchman, B. Theng, D. Righi and B. Delvaux, *Clay Minerals*, 2006, **40**, 383.
11. P. Yuan, P. D. Southon, Z. Liu, M. E. R. Green, J. M. Hook, S. J. Antill and C. J. Kepert, *The Journal of Physical Chemistry C*, 2008, **112**, 15742-15751.
12. Y. Lvov, W. Wang, L. Zhang and R. Fakhrullin, *Advanced Materials*, 2016, **28**, 1227-1250.
13. M. Hanif, F. Jabbar, S. Sharif, G. Abbas, A. Farooq, M. Aziz and J. Churchman, *Clay Minerals*, 2016, **51**, 469-477.
14. M. Liu, Y. Chang, J. Yang, Y. You, R. He, T. Chen and C. Zhou, *Journal of Materials Chemistry B*, 2016, **4**, 2253-2263.
15. Y. Zhang, X. He, J. Ouyang and H. Yang, *Scientific Reports*, 2013, **3**, 2948.
16. M. Makaremi, R. T. De Silva and P. Pasbakhsh, *The Journal of Physical Chemistry C*, 2015, **119**, 7949-7958.
17. E. Nyankson, O. Olasehinde, V. T. John and R. B. Gupta, *Industrial & Engineering Chemistry Research*, 2015, **54**, 9328-9341.
18. J. Jin, L. Fu, H. Yang and J. Ouyang, *Scientific Reports*, 2015, **5**, 12429.
19. A. Hagfeldt, G. Boschloo, L. Sun, L. Kloo and H. Pettersson, *Chemical Reviews*, 2010, **110**, 6595-6663.
20. S. Thomas, T. G. Deepak, G. S. Anjusree, T. A. Arun, S. V. Nair and A. S. Nair, *Journal of Materials Chemistry A*, 2014, **2**, 4474-4490.
21. L.-L. Li, C.-W. Chang, H.-H. Wu, J.-W. Shiu, P.-T. Wu and E. Wei-Guang Diau, *Journal of Materials Chemistry*, 2012, **22**, 6267-6273.
22. T.-L. Hsieh, H.-W. Chen, C.-W. Kung, C.-C. Wang, R. Vittal and K.-C. Ho, *Journal of Materials Chemistry*, 2012, **22**, 5550-5559.
23. V.-D. Dao and H.-S. Choi, *ACS Applied Materials & Interfaces*, 2016, **8**, 1004-1010.
24. H. Seo, M. Shiratani, K. Seneekatima and R. Pornprasertsuk, *Journal of Nanoscience and Nanotechnology*, 2016, **16**, 3332-3337.
25. T.-T. Duong, J.-S. Choi, A.-T. Le and S.-G. Yoon, *Journal of The Electrochemical Society*, 2014, **161**, H166-H171.
26. P. Sudhagar, S. Nagarajan, Y.-G. Lee, D. Song, T. Son, W. Cho, M. Heo, K. Lee, J. Won and Y. S. Kang, *ACS Applied Materials & Interfaces*, 2011, **3**, 1838-1843.
27. L. Y. Han, N. Koide, Y. Chiba, A. Islam, R. Komiya, N. Fuke, A. Fukui and R. Yamanaka, *Appl Phys Lett*, 2005, **86**.

View Article Online
DOI: 10.1039/C7SE00292K

28. J. Bisquert and I. Mora-Sero, *J Phys Chem Lett*, 2010, **1**, 450-456.
29. T. Lopes, L. Andrade, F. Le Formal, M. Gratzel, K. Sivula and A. Mendes, *Physical Chemistry Chemical Physics*, 2014, **16**, 16515-16523.
30. T. Lopes, L. Andrade, H. A. Ribeiro and A. Mendes, *Int J Hydrogen Energ*, 2010, **35**, 11601-11608.
31. P. Sudhagar, A. Devadoss, K. Nakata, C. Terashima and A. Fujishima, *J Electrochem Soc*, 2015, **162**, H108-H114.
32. C. Y. Lee, L. Wang, Y. Kado, M. S. Killian and P. Schmuki, *Chemsuschem*, 2014, **7**, 934-940.
33. D. Song, W. Cho, J. H. Lee and Y. S. Kang, *The Journal of Physical Chemistry Letters*, 2014, **5**, 1249-1258.
34. W. S. Chi, J. W. Han, S. Yang, D. K. Roh, H. Lee and J. H. Kim, *Chemical Communications*, 2012, **48**, 9501-9503.
35. A. Apostolopoulou, A. Margalias and E. Stathatos, *RSC Advances*, 2015, **5**, 58307-58315.
36. M.-S. Kang, J. H. Kim, Y. J. Kim, J. Won, N.-G. Park and Y. S. Kang, *Chemical Communications*, 2005, DOI: 10.1039/b412129p, 889-891.
37. E. Ramasamy and J. Lee, *Chemical Communications*, 2010, **46**, 2136-2138.
38. W. Cho, Y. R. Kim, D. Song, H. W. Choi and Y. S. Kang, *Journal of Materials Chemistry A*, 2014, **2**, 17746-17750.

View Article Online
DOI: 10.1039/C7SE00292K

Table of content